5.4 Comparison of Storm Evolution Characteristics: The NWRT and WSR-88D

Pamela Heinselman, David Priegnitz, Kevin Manross, and Richard Adams
Cooperative Institute for Mesoscale Meteorological Studies, OU, Norman, OK 73072

1. INTRODUCTION

Early detection of rapidly developing hazardous storms requires rapid-scan radar. The National Weather Radar Testbed (NWRT) collects data from a 9.4-cm, single-faced, phased array antenna that supports adaptable scanning strategies and volumetrically scans a storm in time scales of seconds instead of several minutes. Such high temporal sampling provides unprecedented opportunity to research rapidly evolving phenomena and improve warning lead-time for severe weather. Another significant advantage of the phased array antenna is the ability for making cross-beam wind, shear, and turbulence measurements (Zhang and Doviak 2006). Other meteorological benefits are considered in Doviak et al. (2001).

The NWRT and PAR became operational in September 2003 and data collected in 2004 and 2005 for engineering tests, weather observations, and system checks helped to stabilize the hardware and software so that estimates of reflectivity, velocity, and spectrum width are comparable to estimates on the Weather Surveillance Radar-1988 Doppler (WSR-88D; Forsyth et al. 2006). Furthermore, Cheong et al. (2006) used some of these data to explore the implementation of refractivity measurements for estimating low-level moisture fields.

This paper is the first to investigate meteorological advantages of the higher temporal sampling capability of the phased array radar (PAR) as compared to the WSR-88D by performing detailed comparative analysis of storm structure and evolution during three severe weather events. In this paper, the comparative analysis addresses the rapid evolution of three storms observed by the PAR in 2006, including a supercell (24 April), a multicell (30 May), and a hail storm (15 August) that produced a three-body scatter spike (e.g., Zrnić 1987; Lemon 1998). In cases where WSR-88D data are unavailable, the analysis focuses on storm evolution only and is accomplished by comparing PAR images at ~5-min intervals (length of VCP-11 scan) to those collected with higher frequency. A more complete version of this paper is available at http://www.cimms.ou.edu/~heinsel.

The paper is organized such that section 2 distinguishes capabilities of the PAR from those of the WSR-88D, while section 3 describes implemented data collection strategies. Section 4 presents the detailed comparative analysis of the three storms and section 5 summarizes our findings.

Corresponding author address:
Pamela Heinselman
National Weather Center, Room 4905
120 David L. Boren Blvd., Norman, OK, 73072.
E-mail: Pam.Heinselman@noaa.gov

2. COMPARISON OF PAR AND WSR-88D

The most significant difference between the PAR and the WSR-88D is the antenna. The WSR-88D's parabolic antenna forms a beam from a feedhorn, whereas the phased array antenna forms a beam from the 4,352 transmit/receive elements. Additionally, in a WSR-88D, the steering of the beam is accomplished mechanically, by rotating and elevating the antenna. By contrast, with a phased array antenna, steering of the beam is done electronically from a stationary phased array. In general terms, the steering of the beam in azimuth and elevation is controlled by the phasing or on-off timing of the 4,352 transmit/receive elements.

Although the PAR and WSR-88D have different antennas, these radars share three similarities: wavelength (9.4-cm vs 10-cm, respectively), range resolution (both 250 m), and the PAR can mimic WSR-88D VCP tilts and collect data at similar Nyquist frequencies. Because the Phased Array is a 37-year old research radar developed initially for military purposes, it is quite different from the 88-D in several ways. First, because data are collected over a 90 degree sector, volume updates are a minute or less (depending on sector size, etc.). This

means data collection may be focused on specific storms of interest. Second, the PAR was developed with vertically polarized electromagnetic waves in order to track military missiles and airplanes, rather than to detect weather echo. Third, the beam width varies with azimuth. At zero degrees azimuth, or in the direction perpendicular to the array, the beam width is 1.5°. Beam width increases to 2.1 degrees within ± 45° of the zero degree azimuth.

Some surveillance capabilities of conventional radars, like the WSR-88D, are limited compared to capabilities of the PAR. In conventional radars, the beam is shaped and directed by the antenna's reflective surface and volumetric scanning is driven mechanically by the rotation of the pedestal and the inclination of the antenna. The maximum rotation speed of the pedestal restricts volumetric temporal sampling to two to three min (Zrnić et al. 2007) and makes adaptive scanning of meteorological phenomena and other targets (e.g., aircraft) impractical. Long volumetric updates generated by a rotating antenna deliver spatially incongruous vertical storm structures and reduced data quality due to smearing of the beam.

In the PAR, agile electronic steering produces a beam that is shaped and directed electronically from an antenna that remains stationary during data collection. Accordingly, the time required for volumetric updates is reduced, vertical storm structure is more realistic, and smearing of the beam is absent. Although these data quality improvements may result in more accurate and timely algorithm performance and earlier detection and warning of hazardous weather, this paper demonstrates the detailed storm structure and evolution revealed by higher temporal sampling.

The PAR at the NWRT in Norman, Oklahoma has a single-panel array from which the beam is steered within ± 45° from the axis normal to its antenna. Hence, volumetric sampling is on the order of seconds rather than minutes. For example, PAR performs a volume coverage pattern (VCP)-12 with an update of 58 s. Since the WSR-88D scanning strategies are based on a continuously rotating antenna, more detailed scanning of weather and other targets within the volume are not possible. However, with a PAR, electronic steering of the beam supports adaptive scanning of weather and other targets. Thus, the dwell may be based on the time- and space-scale of a particular weather phenomena and its distance from the radar, rather than on mechanical constraints. Furthermore, close to the radar (< 45 km), where conventional VCPs may undershoot storm top, higher elevations may be added to a scanning strategy. The PAR's adaptive scanning capability will be emulated during data collection in spring 2007.

3. DATA COLLECTION

The scanning strategies used for each of the three events described herein were chosen based on storm size and proximity to the PAR. On 24 April and 30 May 2006, a flavor of the VCP 12 scanning strategy was chosen for comparison with the Twin Lakes (KTLX) radar, located ~20 km to the northeast of the PAR. To scan the three supercells that developed southwest of PAR on 24 April, a 90° sector was required, whereas a 20° sector was adequate for the 30 May storms located about 150 km north-northwest of the PAR. These scanning strategies resulted in volumetric updates of ~58 s on 24 April and ~18s on 30 May. Corresponding KTLX data were collected using VCP-12.

A different scanning strategy was used on 15 August that focused on observing the tops of "close" (~40 km west-southwest of the PAR) storms by adding additional elevation angles. Specifically, a 12 pulse, 31 level (up to 41° elevation), short PRT (831 μs) scan strategy with 90° azimuthal coverage and 26 s volumetric updates was used to sample the hail storm examined in section 4. The relatively low number of pulses restricts in-depth analysis of this hail storm to its reflectivity characteristics. Unfortunately, KTLX data were unavailable for this event.

The meteorological advantages stemming from detailed analysis of these rapidly-scanned storms are shown in the next section.

4. ADVANTAGES OF HIGHER TEMPORAL SAMPLING

This section describes unique radar characteristics observed by the PAR during the evolution of three storms. Sampling differences between the PAR and WSR-88D are illustrated and addressed in detail only for the 24 April and 30 May storms because KTLX was unavailable during the 15 August storm.

4.1 *24 April 2006*

On 24 April 2006 conditions were favorable for supercell development near central Oklahoma, well within range of PAR. Severe storms southwest of the PAR were sampled continuously between 2000 UTC on the 24th through 0300 UTC on the 25th. Several supercells were sampled, including a tornado-warned storm, but none produced a confirmed tornado. This event provides a unique comparison between KTLX and PAR as both radars scanned the same storms in southwest OK using similar scanning strategies (as described in section 2).

Characteristics of the 0.5° elevation radar reflectivity and velocity fields were analyzed for a re-intensifying supercell storm located within 60 km of PAR (Fig. 1). During the period of approximately one WSR-88D VCP-12 volume scan (005515–005928 UTC), the supercell underwent significant evolution. The north-northeastward movement of thunderstorm outflow (produced by the rear flank downdraft) toward the storm-relative inflow created an area of developing low-level convergence (Fig. 1b–d) and rotation (Fig. 1e–g) located approximately 50 km southwest of PAR (~ 70 km southwest of KTLX; Fig 1).

Both KTLX and PAR capture the strengthening thunderstorm gust front (convergence), depicted by increasing in-bound velocity to the southwest and south of an area of out-bound velocity. The PAR volume scan update time of ~58 s provided an earlier signal of increasing velocity magnitude and spatial contraction of the inbound/outbound convergence signature (Fig. 1b–d), as well as the developing cyclonic rotation (Fig. 1e–g), than KTLX with its ~213 s volume scan update (Fig. 1a and 1h). Additionally, PAR's faster volume update captured the onset of divergent outflow produced by the forward flank downdraft earlier than the WSR-88D (Fig. 1e).

Another impact of rapid volume scan updates is the ability to view better the inflow of air into the storm's forward flank (near zero velocities located along the northwestward-pointing arrow in Fig. 1a). The rapid updating of volumetric Doppler radar data also allows the user to closely monitor the vertical structure of velocity within a storm, such as the intensification or decay of a mesocyclone or tornado vortex signature (not shown).

4.2 *30 May 2006*

During the early afternoon, a line of severe storms developed over south-central Kansas, along and just ahead of a quasi-stationary front. Outflow produced by these storms initiated new convection over northern Oklahoma. The strongest of these storms, eventually located just northwest of Enid, OK, caught the attention of the Norman WFO, who issued a severe thunderstorm warning at 2227 UTC. Near this time, data collection on this multicell storm and other nearby storm development began at the NWRT. As noted in section 3, because the multicell was located about 150 km from PAR, data were collected with a 20° sector-version of VCP-12 that scanned a full volume every 18 s.

Over an eight minute period, differences in storm evolution portrayed by VCP-12 KTLX data versus rapid-scan PAR data are analyzed by comparing time sequences of vertical cross-sections of reflectivity sharing identical coordinates. At the beginning of the eight minute sequence (223457 UTC), the KTLX reflectivity cross-section (Fig. 2a) depicts three storms in various stages: a mature multicell (x = 11–35 km), a growing multicell (x = 35–47km), and a developing single cell (x = 47–55 km). Near the same time (223501 UTC), the PAR reflectivity cross-section shows similar storm structures (Fig. 2b). The higher-resolution radial display of PAR reflectivities (0.25 km (PAR) vs 1 km (KTLX)), results in sharper, more detailed illustration of storm structure. Furthermore, the PAR's higher temporal scanning produces storm features that are more vertically oriented, compared to the WSR-88D.

The PAR's rapid-scanning captured the subsequent evolution of these storms in great detail. During the period of one conventional VCP-12 scan (~4 min; Fig 2b–h), the "cell" at the leading edge of the mature multicell storm (x = 30–35 km) intensified and the resulting high reflectivity core began to elongate downward. Concurrently, as the growing multicell (x = 35–47 km) approached the mature multicell, it deepened, intensified, and began to produce a descending reflectivity core. At 223727 UTC, the appearance of low reflectivity values (~ 15 dB*Z*) above the freezing level (0°C height = 4.2 km MSL based on 1200 UTC OUN sounding) and near the growing multicell (x = 47–50 km) indicated the initiation of yet another new cell. This new cell continued to develop through the end of the first conventional volume scan.

About four minutes into the sequence, KTLX updated. Near the same time, KTLX (223909 UTC) and PAR (223932 UTC) reflectivity cross-sections showed the onset of the multicell merger (x = 33–37 km). The sharp reflectivity gradient (x = 33–35 km), exhibited only in KTLX data, likely resulted from 1-km data processing in range. Although KTLX and PAR cross-sections share the same coordinates, the new cell developing downwind of the maturing multicell (x = 47–50 km) is defined less clearly in the KTLX cross-section.

Within the period of nearly another conventional VCP-12 scan (223932 –224311 UTC), the reflectivity core (> 48 dB*Z*) at the leading edge of the longer-lived, mature multicell (x = 33 km) continued to elongate toward the ground, while the two multicell storms merged (x = 33–37 km; Fig 2j–2p). In the region where the storm merger occurred, lobes of high reflectivity indicative of quickly intensifying updrafts developed. Amid the merging process, the shorter-lived mature multicell (x = 35–45 km) deepened and developed a core of reflectivity values exceeding 60 dB*Z* (Fig. 2j–m). Shortly thereafter, this intense reflectivity core descended (Fig. 2n–p). Furthermore, within this period the newest cell intensified, grew, and began to merge with southeastern part of the merging multicells (x = 47–50 km).

The relative lack of vertical growth and intensification of the newest cell indicated the beginning of the dissipation process of the merged multicell storm.

This in depth analysis of several storms scanned by both the PAR and WSR-88D illustrates the disparity in time-scales of convective evolution and conventional volumetric updates.

4.3 *15 August 2006*

Numerous small convective cells developed during the early afternoon as surface temperatures reached the mid 90's to low 100's south of a weak front located across central Oklahoma. Data collection at the NWRT began shortly after the appearance of the first radar echoes, just to the south of Norman. Recall from section 3 that a 12 pulse, 31 level (up to 41° elevation) short PRT (831 μs) volume scan strategy was used that sampled the tops of "close" storms and completed in ~26 s. Most of the initial cells were short-lived (30 min) and remained below a 7.5-km midlevel capping inversion, evident in the 12-UTC OUN sounding. Weak southerly winds below the capping inversion resulted in a slight northward drift of these cells.

In the late afternoon, near the frontal boundary, one cell broke through the cap and quickly grew to over 14 km in height (Fig. 3). This cell rapidly evolved into a severe storm with reflectivities exceeding 70 dB*Z*. The Norman WFO issued a warning for this storm at 2231 UTC with the main threats of hail and strong outflow winds.

The PAR captured the evolution of this storm very well. Fig. 3 illustrates the evolution of the main cell and the well-pronounced "Three-body Scatter Spike" (TBSS; Zrnić 1987; Lemon 1998), which developed around 2229 UTC. This feature continued and eventually descended with the main reflectivity core until it dissipated around 2244 UTC. The rapid update capability of the PAR provided a clear picture of the storm during its evolution. Correspondingly, the TBSS would have been visible in only a few WSR-88D volumes (using VCP-11 or 12) and its descent through the storms life cycle would not have been as evident.

5. SUMMARY

This study explored the meteorological advantages of unprecedented rapid-scan data collected by the PAR for three severe storms during the spring and summer of 2006. A comparative analysis of storm evolution depicted by the PAR and the WSR-88D illustrates that significant, rapid storm development occurs during the period of a conventional VCP-12 scan. Important features captured only by the PAR were:

- Rapid deepening and intensification of a maturing storm cell
- Merging process in three evolving cells
- Rapid development and descent of a hail core and attendant three-body scatter spike
- Tracking rapid evolution of low-level convergence and rotation

Although WSR-88D data are indispensable for assessing storm severity, this study illustrates the ability of PARs to provide the high-temporal resolution data needed for early detection of significant storm development, hail signatures, convergence, and wind shear. These high-temporal resolution data should aid in short-term forecasting and warnings, though users may be challenged by the rapid influx of data.

6. REFERENCES

Cheong, B. L., R. D. Palmer, T. Y. Yu, C. Curtis, 2005: Refractivity measurements from ground clutter using the National Weather Radar Testbed Phased Array Radar. Preprints, *32nd Conf. on Radar Meteorology*, Albuquerque, NM, Amer. Meteor. Soc., CD-ROM, P1R.10.

Doviak, R. J., D. S. Zrnic, A. Shapiro, 2001: Phased array weather radar-benefits and challenges. Preprints, *30th Int. Conf. on Radar Meteorology*, Munich, Germany, Amer. Meteor. Soc., 202–204.

Forsyth, D. E., J. F. Kimpel, D. S. Zrnic, R. Ferek, F. Heimmer, T. McNellis, J. E. Crain, A. M. Shapiro, R. J., Vogt, and W. Benner, 2006: Status report on the National Weather Radar Testbed (Phased-Array). Preprints, 22nd *Int. Conf. on Interactive Information and Processing Systems (IIPS)*, Atlanta, GA, Amer. Meteor. Soc., CD-ROM, 11.1.

Lemon, L. R., 1998: The radar "Three body scattered spike": An operational large-hail signature. *Wea. Forecasting*, **13**, 327–340.

Zhang, G., and R. J. Doviak, 2006, Weather radar interferometry to measure crossbeam wind, shear and turbulence. *J. Atmos. Oceanic Technol.*, accepted.

Zrnić, D. S., 1987: Three-body scattering produces precipitation signature of special diagnostic value. *Radio Sci*., **22**, 76–86.

7. ACKNOWLEDGEMENTS

We acknowledge the support of our various organizations in funding and helping to implement this national facility. This paper was funded by NOAA/Office of Oceanic and Atmospheric Research under NOAA-University of Oklahoma Cooperative Agreement #NA17RJ1227, U.S. Department of Commerce (DOC). The statements, findings, conclusions, and recommendations are those of the authors and do not necessarily reflect the views of NOAA or the U.S. DOC. For this paper, we especially thank the leadership of Doug Forsyth and the work of Mark Benner, Dan Suppes, Kurt Hondl, and John Thompson, who kept data collection, archiving, and data display going.

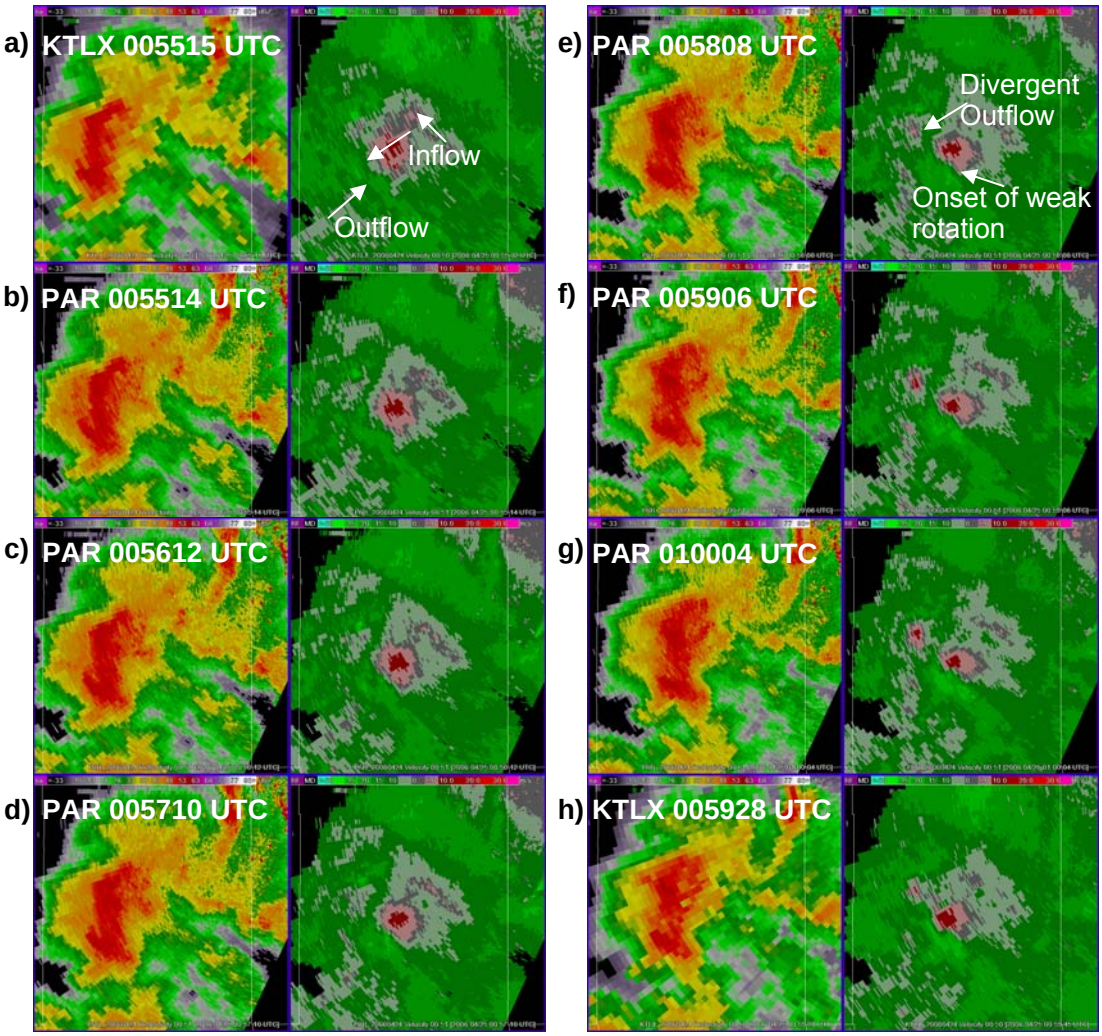

Figure 1. Development of low-level convergence and rotation within a severe thunderstorm near Norge, OK (approximately 50 km from PAR) on 25 April 2006. The top left and bottom right panels are consecutive 0.5° elevation scans from KTLX. The panels in between are consecutive 0.5° elevation scans from PAR. There are 213 s between KTLX scans and 58 s between PAR scans. North is located at the top of each image. Note in b–g the detailed development of the gust front depicted by increasing in-bound (green) velocity to the south-southwest of the out-bound (red) velocity and, in e–g, 1) the development of rotation on the southeast-side of the convergence zone and 2) the intensification of divergent outflow from the forward-flank downdraft.

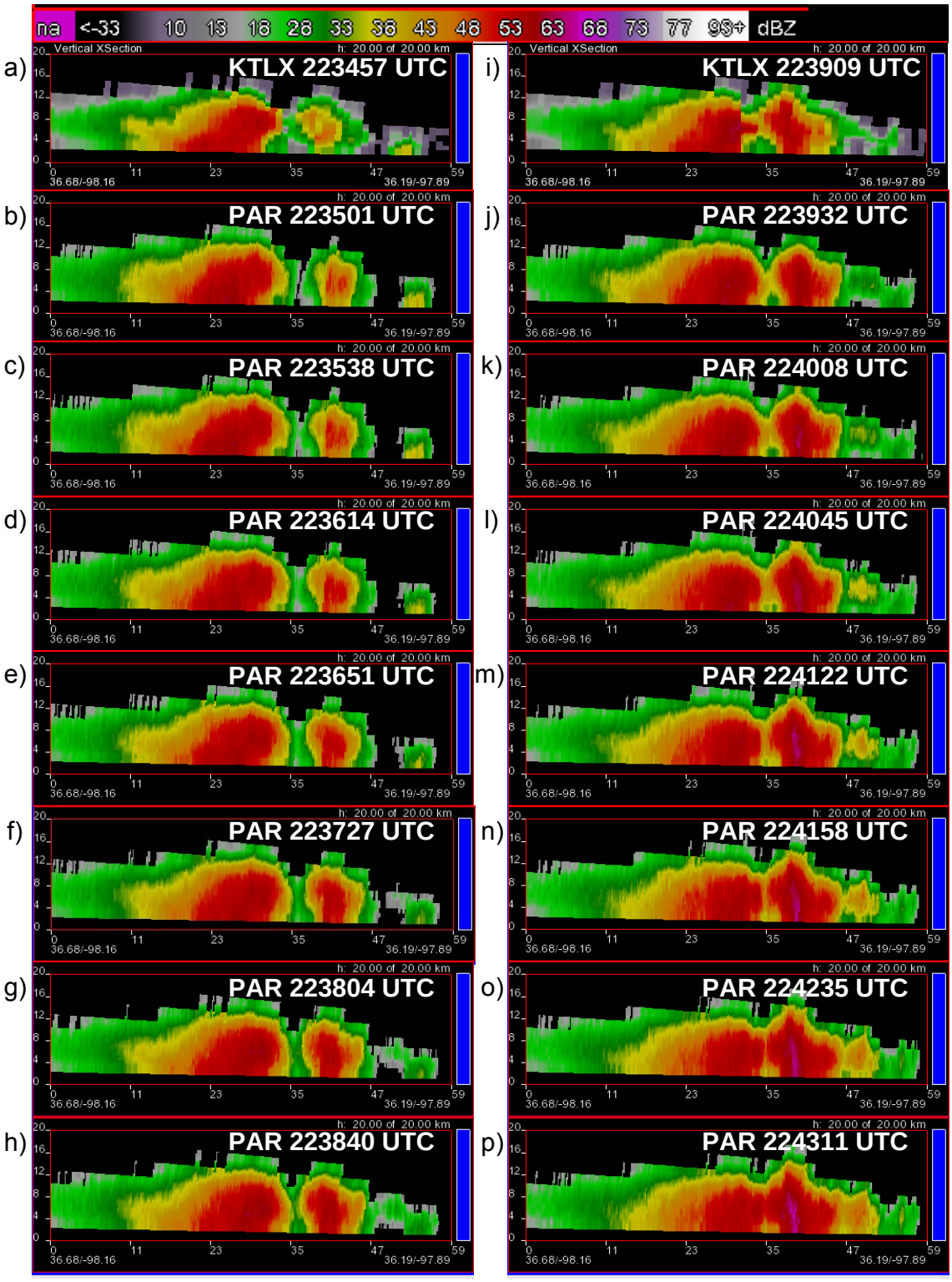

Figure 2. Time sequence of vertical cross-sections of reflectivity through a multicell (x = 11–35 km), a strong, growing cell (x = 35–47 km), and a few weaker cells (x = 47–59 km). The vertical and horizontal scales are in km. Initially the center of the multicell is located about 150 km to the north-northwest of PAR and moves toward the south-southeast at ~13.4 m s^{-1}. The image at the top of each column shows the WSR-88D cross-section (a and i), while the subsequent images (b–h and j–p) show the rapid evolution (images shown every 36 s) of the storms in between (b–h) and subsequent to (j–p) WSR-88D volume scans.

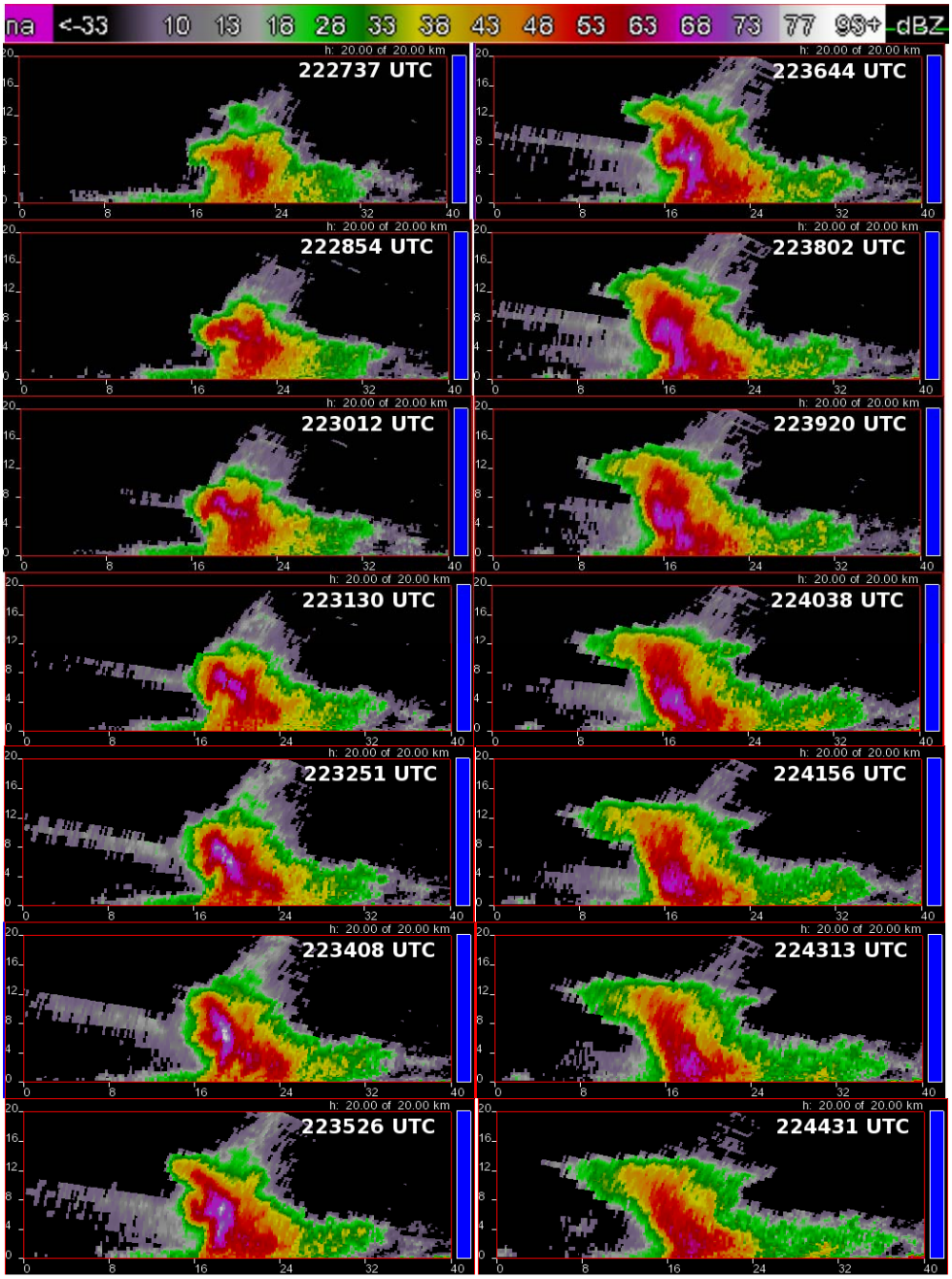

Figure 3. Time sequence of vertical cross-sections of reflectivity thorugh a severe storm on 15 August 2006 as seen by the PAR. The vertical and horizontal scales are in km. The center of the storm is approximately 40 km from the PAR. The freezing level is at ~4.5 km and the -20°C level is at ~8.1 km (based on 12-UTC OUN sounding).